

# A Density Matrix Renormalization Group Method Study of Optical Properties of Porphines and Metalloporphines

Manoranjan Kumar<sup>1,2</sup>, Y. Anusooya Pati<sup>1</sup>, and S. Ramasesha<sup>1</sup>

<sup>1</sup>Solid State and Structural Chemistry Unit,  
Indian Institute of Science, Bangalore 560012, India,

<sup>2</sup>Department of Chemistry, Princeton University,  
Princeton, New Jersey 08544, USA

(Dated: August 4, 2011)

The symmetrized Density-Matrix-Renormalization-Group (DMRG) method is used to study linear and nonlinear optical properties of Free base porphine and metallo-porphine. Long-range interacting model, namely, Pariser-Parr-Pople (PPP) model is employed to capture the quantum many body effect in these systems. The non-linear optical coefficients are computed within correction vector method. The computed singlet and triplet low-lying excited state energies and their charge densities are in excellent agreement with experimental as well as many other theoretical results. The rearrangement of the charge density at carbon and nitrogen sites, on excitation, is discussed. From our bond order calculation, we conclude that porphine is well described by the 18-annulenic structure in the ground state and the molecule expands upon excitation. We have modelled the regular metalloporphine by taking an effective electric field due to the metal ion and computed the excitation spectrum. Metalloporphines have  $D_{4h}$  symmetry and hence have more degenerate excited states. The ground state of Metalloporphines show 20-annulenic structure, as the charge on the metal ion increases. The linear polarizability seems to increase with the charge initially and then saturates. The same trend is observed in third order polarizability coefficients.

## I. INTRODUCTION

The electronic structure of porphyrin and metalloporphyrins has been the subject of extensive study both because of their interesting optical properties and chemical activity [1]. Metalloporphyrins are biologically important molecules, particularly those containing Fe (in Haemoglobin) and Mg (in chlorophyll) ions. The carbon atoms that form the conjugated back-bone undergo easy substitution leading to a large class of porphyrin system with interesting electronic and chemical properties. The  $\pi$ -conjugation present in these molecules gives rise to large nonlinear optic (NLO) responses, which can be tuned by peripheral substitution. Porphyrins are potentially useful in applications such as 3-D optical memory devices [2] and optical power limiting [3]. Solid porphyrins are porous and could find use as molecular sieves and shape selective catalyst [4]. Porphyrins are chemically and photochemically stable and are being used in photo-dynamic therapy [5] and antiviral therapy. Oxo-Vanadium(IV) porphyrins are studied for their anti-HIV properties [6]. Efforts are being made to fabricate solar cells with porphyrin based materials [7], since porphyrin framework is found in chlorophylls. Closely related to porphyrins are the phthalocyanines (Pc), which have a central porphyrinic core. The Pc system has attracted a great deal of attention in recent years for both organic electronic and spintronic applications [8–11]. They have the interesting property of being adsorbed on metal surfaces in a flat orientation. Scanning tunneling microscopic studies have been able to measure spin and charge densities at various positions in the molecule.

Most of the important properties of porphyrins are

dictated by their electronic structure. Hence, electronic structure of porphyrins and metalloporphyrins have been studied by many groups over several decades. Early studies by Goutermann employed a four orbital model to explain the nature of the  $Q$  band (the low-frequency weak absorption band) and the Soret ( $B$ ) band (the high frequency intense absorption band) observed in porphyrins [12]. Weiss *et al.* used the mean field results of Pariser-Parr-Pople (PPP) model Hamiltonian to explain the nature of  $Q$  and  $B$  bands of porphyrins [13]. Christoffersen *et al.* have carried out *ab initio* calculation to study the electronic spectra of porphyrins, metalloporphyrins and other substituted porphyrins [14]. Zerner *et al.* showed that the Soret band is degenerate with parallel polarization with respect to  $Q$  band, using random phase approximation within the intermediate neglect of differential overlap (INDO) method [15]. Using density functional theory, Ruth *et al.* have studied the singlet and triplet spectra of Zn-porphyrin and related compounds and showed that the  $B$  band consists of multiple absorption bands [16].

Several groups have computed the NLO properties of modified porphyrins. Priyadarshy *et al.* [17] obtained the first hyperpolarizability of porphyrin bridged donor-acceptor molecules, wherein, the donor and acceptor molecules are attached at the meso-position. Albert *et al.* [18] have shown that large 2<sup>nd</sup> order NLO response coefficients can be obtained by attaching a donor group at  $\beta$  position and an acceptor group at meso-position; this is expected to increase the difference in the dipole moment between ground and excited states, leading to large first order polarizability. Shirk *et al.* have studied the optical limiting properties of lead phthalocyanine

[19]. Two-photon absorption (TPA) cross section of porphyrin and Zn-porphyrins have been studied by a three state model by Zhou *et al.* [20]. Effect of donor-acceptor strengths on TPA cross section of aggregates of asymmetric Zn-porphyrins have been studied by Ray *et al.* [21].

Porphyrin molecule is a fairly large system and hence is not amenable to accurate ab-initio studies. However, most of the interesting properties of porphyrin are associated with the  $\pi$ -system. Thus the electronic properties of porphyrins can be modeled by employing the well known PPP model for the  $\pi$ -electrons. The Porphyrinic  $\pi$ -system consists of 24 orbitals in conjugation occupied by 26 electrons. Even though the Fock space of the system is finite ( $4^{24} = 2^{48} \sim 2.8 \times 10^{14}$ ), the large Hilbert space of porphine, prohibits doing an exact quantum many body calculation. Specializing to desired total spin and occupancy still leaves the Hilbert space dimension to be very large ( $9.27 \times 10^{11}$ ). Approximate techniques such as restricted configuration interaction (CI) for a few low-lying states is not very reliable, since it relies on cancellation of errors, as in single CI. Thus it is important to bring to bear novel and accurate methods for important low-lying states as well as NLO response coefficient of the systems.

In this paper, we have employed the Density Matrix Renormalization Group (DMRG) method to carry out reliable model many-body calculations of the ground and excited state properties. In the next section we give a brief introduction to the DMRG method. In section III, we discuss the model Hamiltonian and implementation of the DMRG method to porphines. In section IV, we present our results on the properties of the low-lying states of porphine. In section V, we discuss the dynamic nonlinear optic coefficient computed for the system.

## II. INTRODUCTION TO THE DMRG METHOD

The DMRG algorithm involves efficient and accurate ways of truncating the insignificant degrees of freedom from the Fock space of the system. The DMRG method proceeds as follows. Given a model many body Hamiltonian  $\hat{H}$  which we wish to solve for a system with total number of sites  $N$ . We start with a small lattice of  $2L$  sites and obtain the Hamiltonian matrix of this lattice in the real space basis. We obtain by standard methods, the lowest or the desired eigenstates of the Hamiltonian matrix. From the eigenvector we construct the density matrix  $\rho$ , of the subsystems with  $L$  sites by integrating out the states of the remaining  $L$  sites. The matrix elements of the density matrix,  $\rho_{s,s'}^{k,L}$  of the  $L$  sites block in the  $k^{th}$  eigenstate is given by,

$$\rho_{s,s'}^{k,L} = \sum_e C_{s,e}^k C_{s',e}^k \quad (1)$$

where the  $k^{th}$  eigenstate of the  $2L$  sites problem is expressed as

$$\psi_{k,2L} = \sum_s \sum_e C_{s,e}^k |s\rangle |e\rangle, \quad (2)$$

with  $|s\rangle$  and  $|e\rangle$  being the Fock space basis states of the system and environment blocks respectively and  $C_{s,e}^k$  are the associated coefficients. The density matrix  $\rho^{k,L}$  is diagonalized and eigenvectors corresponding to  $m$  dominant eigenvalues of  $\rho^{k,L}$  are used to span the Fock space of the system block. If the order of the matrix  $\rho^{k,L}$  is  $M \times M$ , then the  $m \times M$  matrix  $O$  formed from  $m$  eigenvectors as columns of the  $O$  is used for transforming all the operators of the system block,  $L$ , from the full Fock space to the truncated density matrix eigenvector basis. Thus if  $A$  is an  $M \times M$  matrix of an operator  $\hat{A}$  defined over the  $M$  dimensional Fock space of the system block, then  $\tilde{A} = OAO^\dagger$  gives the renormalized  $m \times m$  matrix representation of  $\hat{A}$ . By interchanging the environment and system blocks, we also obtain renormalized matrix representation of all the operators in the former environment block.

We now add two new sites to the  $2L$  size system at a convenient part of the system, usually in the middle. Using as basis functions, the direct product of the density matrix eigenvectors of the two blocks of the  $2L$  system and the Fock states of the new sites, we can obtain a matrix representation of the  $2L + 2$  site Hamiltonian. From the desired eigenstate  $\psi_{k,2L+2}$  we obtain the density matrix  $\rho^{k,L+1}$  for the two blocks of size  $(L + 1)$  of the augmented  $(2L+2)$  site system and proceed as before to obtain all the renormalized operators on the  $(L + 1)$  sites and iterate until the desired system size is reached. This algorithm of constructing the system is called the infinite DMRG algorithm. In this algorithm, from the eigenvectors at any system size, we can also obtain expectation values of any operator of interest. If the operator consists of product of site operators of different sites in the same block, then we need to carry through matrix representation of the product by renormalizing it at each step and use the renormalized matrix to compute the desired expectation value. If on the other hand the operator is a product of site operators of different sites on different blocks, we can use the renormalized matrix representation of the individual site operators to compute the expectation values. It is possible to target more than one low-lying state simultaneously in a DMRG procedure. This is carried out by computing the density matrix for each desired states separately and using the dominant eigenvectors of an appropriately averaged density matrix of these states. The choice of common DMRG basis for different states permits computing matrix elements such as transition dipoles between states. To access higher excited states of interest such as the  $1^1B_u$  states in polyenes, we need to employ symmetrized DMRG procedure and compute the desired excited state as a low-lying state in an appropriate symmetry subspace. For example, we could access a triplet



is  $(r_{ij} - 1.397) \text{ \AA}$  where  $r_{ij}$  is the length of the bond between atoms  $i$  and  $j$ .

The term  $H_2$  in the PPP Hamiltonian incorporates on-site electron-electron repulsion energy and this corresponds to Hubbard interaction. The Hubbard parameter  $U_i$  is the energy cost for creating double occupancy of the orbital  $i$ . For carbon we have taken the standard value of 11.26 eV. The terms in  $H_3$  correspond to on-site coulombic interaction between electrons in orbitals  $i$  and  $j$ , and we introduce local chemical potential  $z_i$  which is the occupancy of the orbital  $i$  that leaves the  $i^{\text{th}}$  site electronically neutral. The value of  $z$  for C is always 1 while that of nitrogen depends upon the occupancy of the orbital involved in conjugation, for the aza-nitrogen which contributes one electron to the  $\pi$ -conjugation,  $z$  is 1, while for the pyrrole nitrogen which contributes two electrons to the  $\pi$ -conjugation,  $z$  is 2;  $V_{i,j}$  is calculated using Ohno parametrization [34].

We have parametrized  $\epsilon$  and  $U$  for nitrogen atom to fit the experimental excitation gaps and corresponding transition dipole moments for singlets in free base porphine. The parameters which give the best fit are as follows: for aza nitrogens,  $\epsilon_{N_5} = \epsilon_{N_{20}} = -3.20 \text{ eV}$  and  $U_{N_5} = U_{N_{20}} = 12.34 \text{ eV}$ ; for pyrrole nitrogens,  $\epsilon_{N_{12}} = \epsilon_{N_{13}} = -14.0 \text{ eV}$  and  $U_{N_{12}} = U_{N_{13}} = 15.00 \text{ eV}$ . The value of  $t_{CN}$  is taken to be  $-2.3 \text{ eV}$  and  $-2.4 \text{ eV}$  for C – N single and double bonds respectively. Other transfer integrals calculated from Eq. 4 are shown in Fig. 1. The nitrogen parameters reflect the more compact  $2p$  orbitals of nitrogen compared to  $2p$  orbitals of carbon.

We have employed the DMRG methods to study the ground state (gs) and low-lying states of porphine. The topology of the transfer terms in porphines is not strictly one dimensional. The porphine system can be built up from a 4-site ring, by adding two sites at a time, in many different ways. The scheme shown in Fig. 2 provides a highly accurate scheme for building up the porphine framework, besides retaining the symmetries of porphine at every stage of the DMRG implementation. We have also carried out finite DMRG sweeps to improve the accuracy. The accuracy of the DMRG scheme is benchmarked against Hückel model results for the system. In the DMRG studies, we have retained 210 density matrix eigenvectors (DMEVs) and carried out two finite DMRG sweeps. The order of the Hamiltonian matrix is about 45,000 after using two symmetries, namely, spin invariance and  $C_2$  symmetry. The matrix is sparse and symmetric. We obtain a few low-lying states of the matrix using Davidson algorithm. Various properties such as charge and spin densities and b.o.s in different eigenstates can be computed since the matrices of the creation operators, the occupation number operators of all the sites and the b.o operators of all the bonds are renormalized at every step.

In the molecular systems with strong electron correlations, it is difficult to identify the desired excited states such as two photon states or optically allowed excited

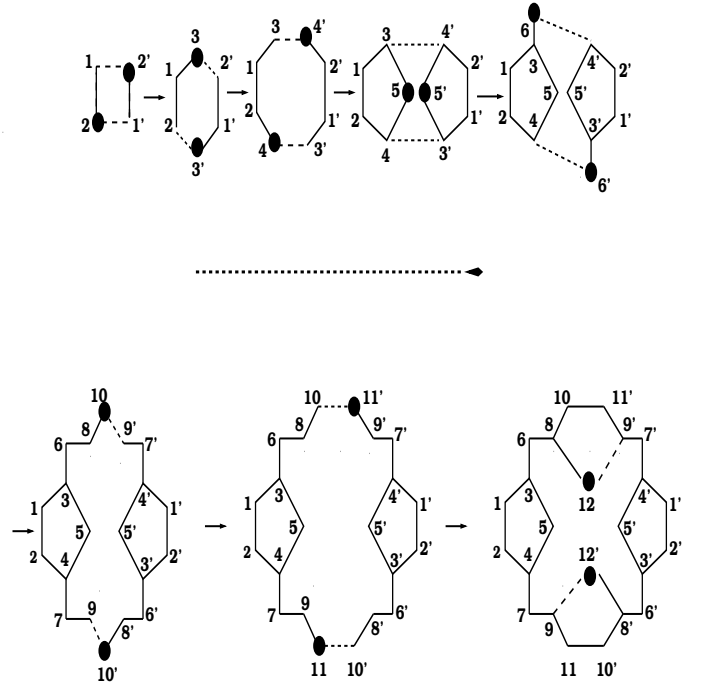


FIG. 2: A highly accurate scheme for building the porphine structure for DMRG calculations. At every step of the DMRG algorithm, we add two new sites shown by filled circle. Positive integers correspond to the sites of the left block and negative integers to the sites of the right block.

states, unless symmetry is exploited. The Hamiltonian is spin conserving, however, exploiting the conservation of both  $S^2$  and  $S^z$  ( $S$  corresponds to total spin) within a DMRG scheme is difficult. Instead we have used spin invariance symmetry and  $S^z$  conservation, to reduce the dimensionalities of the spaces. Spin invariance symmetry corresponds to invariance of the Hamiltonian when all the spins are rotated by  $\pi$  around the y-axis, within the  $M_s = 0$  ( $M_s$  is eigenvalue of  $S^z$  operator) subspace. The spin invariance operator divides the basis into two subspaces, one of even total spin and another of odd total spin. The spatial symmetry we have employed is the  $C_2$  symmetry, even though the molecule has  $D_2$  symmetry. The  $C_2$  axis chosen by us passes through the center of the molecule and is perpendicular to molecular plane. The spin invariance symmetry commutes with the  $C_2$  symmetry and the resulting group has four one dimensional representations. Optical transitions are from states which are even under  $C_2$  symmetry to those that are odd, and retain total spin. The triplet ( $S=1$ ) state is targeted as the lowest state in the  $M_s = 1$  sector. Since we are dealing with a nonzero  $M_s$  subspace, the spin invariance symmetry does not exist in this case and we only employ the spatial symmetry. Besides, for computing properties such as transition dipoles and dynamic linear and non-linear polarizabilities, we need to express states in the different symmetry subspace by using the same DMRG

basis states. In order to retain proper balance of various states, we construct an average density matrix, averaged over density matrices of several low-lying states in each subspace and employ dominant eigenvectors of the averaged density matrix. The dynamic nonlinear optics response coefficient are computed using correction vector (CV) technique [35].

Conventional frequency dependent linear and nonlinear optical coefficient calculations rely on the knowledge of transition dipole moments between the gs and all excited states. For exact calculation of NLO properties, the sum over states (SOS) method is most widely used. Generally, between 30 to 100 excited states, computed within a restricted CI scheme are used to obtain NLO coefficients. Soos and Ramasesha [36] introduced the CV method for calculating NLO coefficients within an exact diagonalization scheme which incorporates the contribution of all higher excited states, without explicitly obtaining the excited state eigenfunctions. In this method, a correction vector (CV) is obtained using the gs wavefunction and the Hamiltonian matrix. CV method involves computation of the first and second order correction vectors  $\phi_i^{(1)}(\omega_1)$  and  $\phi_{ij}^{(2)}(\omega_1, \omega_2)$ , which are defined as,

$$(\mathbf{H} - E_G + \hbar\omega_1 + i\Gamma)|\phi_i^{(1)}(\omega_1)\rangle = \tilde{\mu}_i|G\rangle \quad (5)$$

$$(\mathbf{H} - E_G + \hbar\omega_2 + i\Gamma)|\phi_{ij}^{(2)}(\omega_1, \omega_2)\rangle = \tilde{\mu}_j|\phi_i^{(1)}(\omega_1)\rangle \quad (6)$$

where  $\mathbf{H}$  is the Hamiltonian matrix in the chosen many-body basis,  $E_G$  is the gs energy,  $\omega_1, \omega_2$  are the excitation frequencies and  $\tilde{\mu}_i$  is the  $i^{th}$  component of the dipole displacement operator, ( $\tilde{\mu}_i = \hat{\mu}_i - \langle G|\hat{\mu}_i|G\rangle$ ), and  $\Gamma$  is the average lifetime of the excited states. It can be shown that  $\phi_i^{(1)}(\omega_1)$  and  $\phi_{ij}^{(2)}(\omega_1, \omega_2)$  when expressed in the basis of the eigenstates of the Hamiltonian  $|R\rangle$  are given by,

$$|\phi_i^{(1)}(\omega_1)\rangle = \sum_R \frac{\langle R|\tilde{\mu}_i|G\rangle}{E_R - E_G + \hbar\omega_1 + i\Gamma}|R\rangle \quad (7)$$

$$|\phi_{ij}^{(2)}(\omega_1, \omega_2)\rangle = \sum_S \sum_R \frac{\langle S|\tilde{\mu}_j|R\rangle \langle R|\tilde{\mu}_i|G\rangle}{(E_R - E_G + \hbar\omega_1 + i\Gamma)(E_S - E_G + \hbar\omega_2 + i\Gamma)}|S\rangle \quad (8)$$

Therefore  $|\phi_i^{(1)}(\omega_1)\rangle$  and  $|\phi_{ij}^{(2)}(\omega_1, \omega_2)\rangle$  can be readily used to compute linear and nonlinear frequency dependent polarizabilities. The third order NLO coefficients corresponding to sum frequency generation, in terms of these correction vectors, are given by,

TABLE I: Comparison of excitation gaps and transition dipole moments between DMRG and exact calculations, in the non-interacting limit. Gaps are given in eV and transition dipoles are in a.u.

DMRG						Exact		
$m = 180$			$m = 210$					
Gap	$ \mu_x $	$ \mu_y $	Gap	$ \mu_x $	$ \mu_y $	Gap	$ \mu_x $	$ \mu_y $
1.67	0.17	2.74	1.65	0.22	2.73	1.50	0.44	2.76
1.82	1.07	0.09	1.78	1.47	0.32	1.56	2.37	0.52
1.96	0.45	2.38	1.95	0.65	2.36	1.80	2.25	0.44
2.05	2.90	0.24	2.03	2.72	0.51	1.87	0.42	2.35

$$\gamma_{ijkl}(-\omega_\sigma; \omega_1, \omega_2, \omega_3, ) = \hat{P}_{ijkl}(\langle \phi_i^{(1)}(-\omega_\sigma)|\hat{\mu}_j|\phi_{kl}^{(2)}(-\omega_1 - \omega_2, -\omega_1)\rangle) \quad (9)$$

where  $\hat{P}_{ijkl}$  generate all permutations of  $(-\omega_\sigma, i), (\omega_1, j), (\omega_2, k), (\omega_3, l)$  leading to 24 terms for  $\gamma$  (with  $\omega_\sigma = \omega_1 + \omega_2 + \omega_3$ ). The linear polarizability components are given by

$$\alpha_{ij}(\omega) = (\langle \phi_i^{(1)}(\omega)|\tilde{\mu}_j|G\rangle + \langle \phi_i^{(1)}(-\omega)|\tilde{\mu}_j|G\rangle) \quad (10)$$

The  $\phi_i$ s are exact within the Hilbert space chosen for the Hamiltonian. The linear algebraic equations that can be solved efficiently by a small matrix algorithm developed by Ramasesha [37].

Ramasesha *et al.* incorporated the CV technique in the DMRG method and have shown it to be robust [38]. In the CV-DMRG procedure, the average density matrix is constructed from a weighted average of the gs and the density matrix constructed from the correction vector. We will concentrate on the spatially averaged values of first and third order optical response. The expression for these are given by,

$$\alpha_{av} = \sum_{i=1}^3 \frac{1}{3} \alpha_{ii} \quad (11)$$

$$\gamma_{av} = \sum_{i,j=1}^3 \frac{1}{15} (2\gamma_{iijj} + \gamma_{ijji}) \quad (12)$$

where  $\{i\}$ s are Cartesian indices (x,y,z).

We have compared our DMRG results for the non-interacting Hamiltonian with exact Hückel MO results for porphine. In the above calculations, at each iteration, the density matrix is constructed as the weighted average of the density matrix of five lowest eigenstates. Table I. compares the optical gaps and transition dipole moments for two different DMRG cut-offs,  $m$ , from finite DMRG calculations with exact results. We observe that  $m = 210$  gives quite accurate results and keeping higher  $m$  increases the demand on computational resources with only marginal improvement in the results. DMRG results

slightly overestimate the higher excited states ( $\approx 0.15 - 0.20$  eV). Due to near degeneracy in the excitation levels, the components of transition dipole moments do not agree very well with Hückel MO calculations although the magnitudes are in good agreement and the qualitative trend is maintained. All the studies that we report in this paper are based on retaining 210 density matrix eigenvectors and two sweeps of the finite algorithm.

#### IV. RESULTS AND DISCUSSION

This section is divided into three subsections. In the next subsection, we discuss results of our study on FBP followed by the metallo-porphine. In the last section, linear and nonlinear optic properties are discussed.

##### A. Free base porphine

We have obtained six lowest lying states in A and B subspaces for singlets as well as triplets of FBP using symmetrized DMRG method. In Table II we present the energies of singlets and in Table III that of triplets. The ground state energy is set to zero, so the energies reported are the excitation gaps from the gs. We have also presented experimental gaps and absorption intensities, wherever available. DMRG results correspond to isolated molecule calculations in the gs geometry. The experimental optical gaps are usually red shifted by about 0.5 eV from the gas phase values. The first peak observed in the optical spectra is at 1.98 eV while that calculated is at 1.66 eV. If we include the red shift of the theoretical gap, the agreement is off by about 0.8 eV. This suggests that the first peak in the spectra may be due to  $n - \pi^*$  transition, and our model being a purely  $\pi$ -electron model cannot account for such a state. The 1.66 eV transition in the solid state would be shifted to about 1 eV corresponding to approximately 1200 nm, and will not be observed in an optical spectra. The 2.86 eV absorption to the  $2^1B$  state is X-polarized (see Table II) while the nearly degenerate  $3^1B$  and  $4^1B$  states at 3.89 eV and 3.91 eV peaks have X and Y polarizations respectively. It should be noted that the low-temperature spectra of the free base porphine shows a split in the  $B$  band with equal intensity and separated by 0.03 eV [40]. Other theoretical studies also show nearly degenerate levels at this energy. The 4.18 eV band ( $5^1B$ ) corresponds to the  $N$  band while the 4.83 eV absorption to  $6^1B$  corresponds to the weak  $L$  band transitions observed in FBP.

In Table III, we give energies of several low-lying triplet states. The lowest singlet-triplet gap in the system is 1.42 eV from our calculations, experimental value is 1.58 eV, which is in fair agreement. The lowest triplet-triplet absorption, from our calculations is found at 1.67 eV, while experimentally two very close triplet-triplet absorption peaks are found at 1.58 eV and 1.65 eV [42, 43]. Our calculations show weak absorption peaks at 2.09 eV and

TABLE II: Excitation gaps of six low-lying excited states and corresponding transition dipole moments compared with the experimental results for optically allowed states. Calculated oscillator strengths are given in parenthesis. Experimental results are from reference [41]. The experimental oscillator strengths are normalized with respect to most intense absorption. Sum of calculated intensity ( $\mu_x^2 + \mu_y^2$ ) for the state 3 and 4 is taken to be unity as they are nearly degenerate and all others are normalized with respect to it. Transition dipole between gs and all excited  $A$  states strictly vanishes by symmetry.

State label	Optical gap (in eV)	$ \mu_x $ (in a.u.)	$ \mu_y $ (in a.u.)	Observed value
$1^1B$	1.66 ( <b>0.16</b> )	0.05	0.30	1.98 ( <b>0.01</b> )
$2^1A$	2.94	-	-	-
$2^1B$	2.86 ( <b>0.26</b> )	0.39	0.05	2.42 ( <b>0.05</b> )
$3^1A$	3.40	-	-	-
$4^1A$	3.53	-	-	-
$3^1B$	3.89 ( <b>1.00</b> )	0.48	0.06	3.33 ( <b>1.00</b> )
$4^1B$	3.91 ( <b>1.00</b> )	0.10	0.59	-
$5^1A$	4.01	-	-	-
$5^1B$	4.18 ( <b>0.21</b> )	0.04	0.35	3.65 ( <b>0.87</b> )
$6^1A$	4.33	-	-	-
$6^1B$	4.83 ( <b>0.01</b> )	0.00	0.07	4.25 ( <b>0.87</b> )

TABLE III: Excitation gaps of low-lying excited states and transition dipole moments in triplet manifolds. Note that all the excitations are from  $B$  to  $A$  space. Experimental results are from references [?] and [43].

State label	Triplet energies (in eV)	T-T gap (in eV)	$\mu_x$ (in a.u.)	$\mu_y$ (in a.u.)	Observed value
$1^3B$	1.42	-	-	-	-
$2^3B$	2.45	1.03	-	-	-
$3^3B$	2.93	1.51	-	-	-
$1^3A$	3.09	1.67	0.00	0.18	1.58
$2^3A$	3.51	2.09	0.03	0.02	1.65
$4^3B$	3.55	2.13	-	-	-
$3^3A$	3.55	2.13	0.05	0.08	-
$4^3A$	4.26	2.84	0.00	0.29	2.82 / 2.96
$5^3B$	4.28	2.86	-	-	-
$5^3A$	4.83	3.41	0.02	0.12	3.23

2.13 eV and a much stronger absorption is predicted at 2.84 eV. Experimentally two absorption peaks are seen at 2.82 and 2.96 eV, close to the theoretical values. Theory also predicts a triplet absorption at 3.41 eV while experimentally a triplet absorption is seen at 3.23 eV. Overall, we find that the DMRG results for the  $\pi$ -electron model are quite consistent with experimental observations.

##### 1. Electron density and bond order analysis

We have analyzed the eigenstates by computing charge densities and b.o.s in various states. In the gs, all  $\beta$  car-

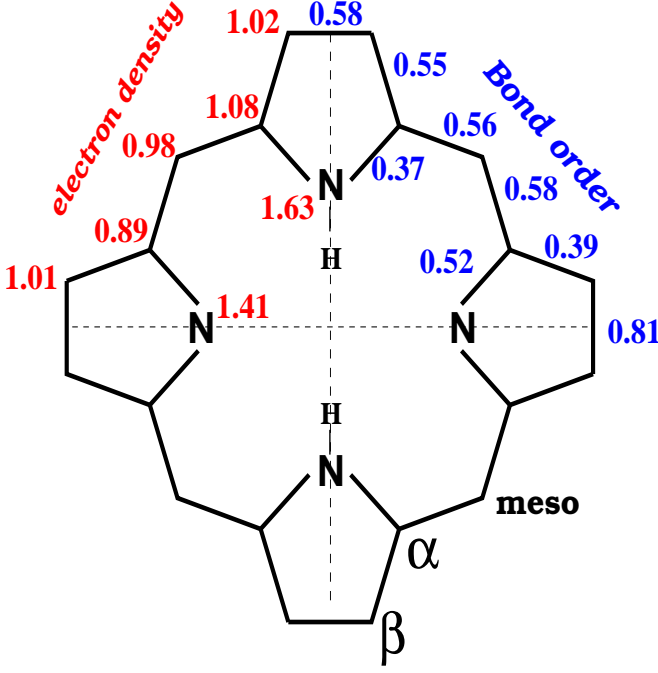


FIG. 3: Electron density and b.o. for the gs of porphine. Charge densities are shown on the left part of the structure while b.o.s are shown on the right part. The site indices and bond indices are given in red and blue, respectively, for half of the system. The  $D_2$  symmetry gives value for remaining sites and bonds of the molecule.

bon atoms have slightly more than one electron. The electron density at  $\alpha$  carbon atoms in aza ring is 0.89 and in pyrrole ring it is 1.08 and have opposite acceptor (donor) tendencies. At *meso*-carbon, the charge density is 0.98. This is consistent with the earlier semi-empirical calculations which show that the  $C_{\text{meso}}$  is electron deficient and  $C_\beta$  is slightly electron rich [18]. Nitrogen in the aza ring has 1.41 electrons and in pyrrole ring it has 1.63 electrons. These results are in agreement with the earlier theoretical work [13]. The gs charge density and b.o. are given in Fig. 3. It is interesting to note that although aza ring nitrogen contributes only one electron to  $\pi$ -conjugation the electron density is 1.41.

For excited states which are Y-polarized, electron density is transferred from nitrogen in aza ring to the neighboring carbon atoms while for the the X-polarized excited state the electron is transferred from the carbon atom to the  $N$  atom. Except for the fourth and fifth excited states, for which there is considerable transition dipole moment, the change in electron density on  $C_\alpha$  and  $C_\beta$  sites are negligible. In the fourth and fifth excited states, there is considerable electron density redistribution between carbon and nitrogen atoms. The electron density at meso sites remain almost the same in all the excited states.

In pyrrole rings the opposite trend of electron transfer is observed except for the sixth excited state. The

TABLE IV: Electron density  $\rho$  for gs and difference of electron density  $\delta\rho$  for the optically allowed states w.r.t. gs.

Site	$\rho$	$\delta\rho$					
	gs ( $A_0$ )	$B_1$	$B_2$	$B_3$	$B_4$	$B_5$	$B_6$
$C_\beta$ (aza)	1.01	0.01	0.00	-0.00	-0.03	-0.04	-0.00
$C_\beta$ (aza)	1.01	0.00	-0.00	-0.01	-0.02	-0.05	-0.01
$C_\alpha$ (aza)	0.89	-0.01	0.01	-0.01	0.04	0.03	0.02
$C_\alpha$ (aza)	0.89	-0.01	0.02	0.01	0.05	0.05	0.01
$N$ (aza)	1.41	-0.02	0.00	0.02	-0.11	-0.08	-0.03
$C_{meso}$	0.98	0.01	0.00	0.03	0.03	0.03	0.01
$C_{meso}$	0.98	0.00	-0.00	0.01	0.02	0.03	0.02
$C_\alpha$ (pyr)	1.08	-0.02	0.04	0.02	-0.03	-0.02	0.04
$C_\alpha$ (pyr)	1.08	-0.01	0.03	0.03	-0.03	0.01	0.02
$C_\beta$ (pyr)	1.02	-0.00	0.04	-0.01	0.00	0.03	-0.00
$C_\beta$ (pyr)	1.02	0.01	0.04	-0.05	0.03	0.02	0.03
$N$ (pyr)	1.63	0.04	-0.19	-0.05	0.06	-0.00	-0.11

TABLE V: Bond orders of gs and difference in b.o. for six low-lying states w.r.t gs, in the singlet manifold are given. Symmetry space of states are given in parentheses.

Bond	b.o	$\Delta(b.o)$	$\Delta(b.o)$	$\Delta(b.o)$	$\Delta(b.o)$	$\Delta(b.o)$	$\Delta(b.o)$
	G.S (1A)	(1 <sup>st</sup> )(1B)	2 <sup>nd</sup> (2A)	3 <sup>rd</sup> (2B)	4 <sup>th</sup> (3A)	5 <sup>th</sup> (4A)	6 <sup>th</sup> (3B)
$C_\beta - C_\beta$ (aza)	0.81	-0.01	-0.01	-0.03	-0.15	-0.16	-0.04
$C_\beta - C_\alpha$ (aza)	0.39	0.00	0.01	0.02	0.10	0.08	0.03
$C_\beta - C_\alpha$ (aza)	0.38	0.00	0.01	0.01	0.11	0.08	0.02
$C_\alpha - N$ (aza)	0.54	-0.01	-0.02	-0.03	-0.06	-0.07	0.00
$C_\alpha - N$ (aza)	0.52	-0.01	-0.01	0.00	-0.02	-0.05	-0.03
$C_\alpha - C_{\text{meso}}$	0.59	-0.03	-0.01	-0.02	-0.10	-0.03	-0.01
$C_\alpha - C_{\text{meso}}$	0.58	-0.03	0.01	0.02	-0.06	-0.02	-0.04
$C_\alpha - C_{\text{meso}}$	0.55	-0.01	-0.02	-0.02	0.02	-0.04	-0.03
$C_\alpha - C_{\text{meso}}$	0.56	-0.01	-0.03	-0.06	0.00	-0.06	-0.01
$C_\alpha - C_\beta$ (pyr)	0.57	-0.01	0.04	0.04	-0.02	0.06	0.02
$C_\alpha - C_\beta$ (pyr)	0.55	-0.01	0.04	0.05	0.00	0.05	0.01
$C_\beta - C_\beta$ (pyr)	0.58	-0.04	-0.12	-0.19	-0.07	-0.14	-0.18
$C_\alpha - N$ (pyr)	0.37	-0.02	-0.06	-0.04	-0.05	-0.06	-0.11
$C_\alpha - N$ (pyr)	0.38	-0.03	-0.03	-0.02	-0.06	-0.04	-0.09

electron is transferred to N when the polarization is in Y direction and is transferred from N, when it is in X direction. The magnitude of electron distribution is maximum in second excited state. In the fifth excited state, there is hardly any change in the electron distribution at N atom, but the charge is transferred between  $C_\alpha$  and  $C_\beta$  atoms. Deviation in electron density from the gs are given in Table IV.

It is known from the literature that the porphyrin can have two conjugation pathways: an inner 18-annulene pathway and an outer 20-annulene pathway (Fig. 4). From our b.o. calculations we find that b.o.s are more uniform ( $0.55 \pm 0.03$ ) along the 18 annulene pathway. We should expect porphine to behave more as an 18-annulene system than a 20-annulene system. The two  $C_\beta - C_\beta$  bonds have much higher bond order (0.81) and hence the 20 annulene description of porphines can be discarded. This structure is in confirmity with X-ray structure [33] as well as other theoretical work by Weiss *et al.* [13]. From Fig. 4, we see that pyrrole N is not strongly in-



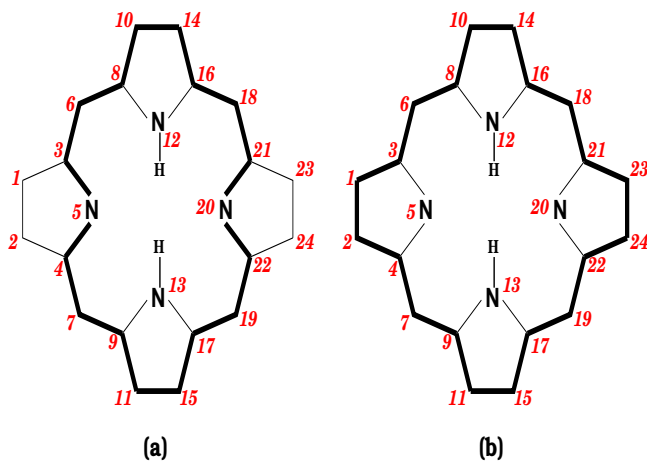


FIG. 4: Two possible equilibrium geometries in gs : (a) 18-sites annulenic structure and (b) 20-sites annulenic structure, shown by bold lines.

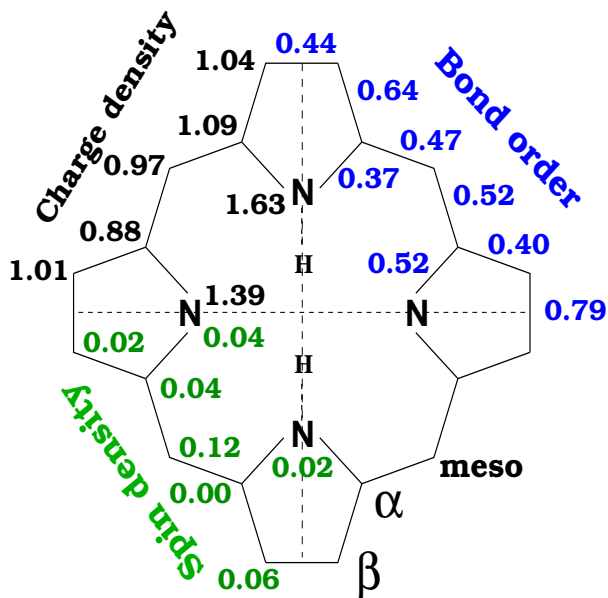


FIG. 5: Electron density, spin density and b.o.s for the lowest triplet state of porphine. Spin and charge densities are shown on the left part of the structure while b.o.s are shown on the right part. The D<sub>2</sub> symmetry gives value for other half of the molecule.

involved in  $\pi$ -conjugation,  $C_\beta - C_\beta$  b.o. is small and hence we expect bond length of  $C_\beta - C_\beta$  in pyrrole rings to be large. In aza rings, N is involved in the  $\pi$ -conjugation path and a reverse trend in b.o. is observed, namely,  $C_\beta - C_\beta$  b.o., is large and we should expect a shorter  $C_\beta - C_\beta$  bond. The  $C_\alpha - C_\beta$  bond length is increased [44] in aza rings.

The deviation from the g.s. bond order is given in Table V. In the first excited state, all the b.o.s become

smaller compared to their values in gs geometry. The change in b.o. is only marginal in aza rings, while in pyrrole rings  $C_\beta - C_\beta$  bonds become weaker. All the three C - C b.o.s are uniform. The C - N bonds also become weaker. The *meso*-bonds connected to aza rings become weaker than those connected to pyrrole rings. Hence we expect the equilibrium geometry in the first excited state to have expansion of the whole  $\pi$ -system.

In the second excited state,  $C_\beta - C_\beta$  bond of aza rings weakens and  $C_\alpha - C_\beta$  bonds become stronger. *Meso* bonds connected to aza rings become weaker and the rest become stronger compared to the 1<sup>st</sup> excited state. The pyrrole ring becomes more pyrrolic, i.e. the  $C_\beta - C_\beta$  b.o. reduces considerably and the  $C_\alpha - C_\beta$  bond becomes a strong bond while the C - N bonds get weaker. This bond pattern is in conformity with the charge distribution in the second excited state. The charge is depleted from the N and accumulated on C atoms. The b.o. pattern of third excited state is similar to that of second excited state.

In the fourth excited state,  $C_\beta - C_\beta$  bonds of aza rings become very weak. The  $C_\alpha - C_\beta$  and the C - N bonds have almost the same b.o. ( $0.49 \pm 0.01$ ). This can again be attributed to the fact that in the fourth excited state, there is charge accumulation on  $C_\alpha$  atoms and depletion at N atom. The bond alternation of the *meso*-bonds reduce. In pyrrole ring, all the three C - C bonds are almost uniform. Note that in both the first excited and 4<sup>th</sup> excited states, there is charge accumulation at pyrrole N and all the three C - C bonds have uniform bond order.

In the fifth excited state, the aza b.o. and charge distribution pattern are same as in fourth excited state. The charge density pattern at pyrrole ring is similar to that of the third excited state and hence the b.o. pattern is similar to that of third excited state, namely alternate single-double-single bond for three C - C bonds and weaker C - N bonds.

In the sixth excited state, the charge depletion at aza N is not significant and the b.o. is slightly alternating for  $C_\alpha - C_\beta$  and C - N bonds. The  $C_\beta - C_\beta$  bond is more like a double bond. The pyrrole ring is less pyrrole like and the C - N bonds become weak.

In aza rings, when the charge is taken away from N, the b.o.s of  $C_\alpha - C_\beta$  bonds and C - N bonds would be uniform. On the other hand, when there is excess charge at N, the bonds alternate. In pyrrole rings, when there is charge accumulation at N, the three C - C bonds become almost uniform and when the charge is taken away from N,  $C_\alpha - C_\beta$  bonds become stronger and  $C_\beta - C_\beta$  bonds become weaker. In all the excited states, either the aza C - N bonds have weak bond alternation or the pyrrole C - N bonds.

Spin densities, charge densities and b.o.s are shown in Fig. 5, in the lowest triplet state of FBP. The electron density on  $C_\beta$  and  $C_\alpha$  carbon atoms are comparable to that in gs while it decreases on the nitrogen atom of aza-rings and remains constant for N atom on pyrrole-rings, compared to gs. At  $C_{\text{meso}}$  sites, electron



density decreases in the lowest triplet state. The values of  $C_\beta - C_\beta$ ,  $C_\alpha - C_\beta$  and  $C_\alpha - C_{\text{meso}}$  b.o.s in the aza-ring are almost same as in gs while  $C_\alpha - C_{\text{meso}}$  and  $C_\alpha - C_\beta$  b.o.s of pyrrole-ring increase while for  $C_\beta - C_\beta$  it decreases.  $C - N$  b.o.s in aza-rings decrease but increase in pyrrole-rings. Spin density values on  $C_\beta$  atoms in aza-ring are small but are relatively higher (0.045) in pyrrole-rings. Spin density values are very high on  $C_{\text{meso}}$  sites (0.16) and nitrogen atom (0.12) in the aza-rings while this value is very small on the nitrogen atom of pyrrole-rings.

## B. Metallo-porphines

Metallic porphines are biologically important molecules. There are two categories of metallic porphines - regular and irregular porphines. In the case of regular porphines, the metals have closed shells and in the latter, they have partially filled shells. Our study concentrates on regular metallic porphines. We have placed the metal ion at the center of the porphine molecule and it acts only as a source of electric field, *i.e.*, we have not taken the overlap of metallic  $d$ - orbitals with porphine  $\pi$ -orbitals. The modified Hamiltonian to account for the effect of the metallic ion is given by,  $\hat{H} = H_{PPP} + \sum q_M(\hat{n}_i - z_i)/r_{M_i}$  where  $q_M$  is charge on the metal and  $(\hat{n}_i - z_i)$  is effective charge operator at site  $i$ ,  $r_{M_i}$  is the distance between metal at the center and  $i^{\text{th}}$  atom. In the presence of the metal ion, pyrrolic  $N$  gets deprotonated and all the four five-membered rings become equivalent and hence the bond alternation observed in the neutral porphine molecule also vanishes. So, we have taken uniform transfer integrals for all the  $C - C$  bonds and a single value of  $\epsilon_N$  and  $U_N$  for all nitrogens. The uniform  $\epsilon_N$  and  $U_N$  used in the Hamiltonian are -7.8 eV and 12.34 eV respectively. We have varied the charge on the metal ion from 1 to 5 and studied the effect of oxidation state of the metal ion on porphine spectra, ground state charge distribution and nonlinear optical properties.

### 1. Ground state charge density and bond orders

Charge densities on porphine for different oxidation states of the central metal ion are given in Table VI. Charge density on the  $C_\beta$  atoms decreases while it increases on  $C_\alpha$  atoms. The charge density on  $N$  atoms increases while those on  $C_{\text{meso}}$  atoms decrease.

Bond orders in gs for metallo-porphine as a function of oxidation state on the metal ion are given in Table VII. As in the FBP molecule,  $C_\beta - C_\beta$  bonds in the aza rings are the strongest bonds except for +5 oxidation state. As the oxidation state of the metal ion increases,  $C_\beta - C_\beta$  bond order decreases and the  $C_\beta - C_\alpha$  b.o.s increase. With the increase in  $q_M$ , as the charge on  $N$  reaches its maximum value, the b.o. of all  $C - N$  bonds

TABLE VI: Charge densities on unique sites of metallo-porphine for different oxidation states of the metal ion.

Site	Charge on metal site					
	0	1	2	3	4	5
$C_\beta$ (aza)	1.01	1.04	0.99	0.94	0.87	0.80
$C_\alpha$ (aza)	0.89	0.79	0.82	0.88	0.96	1.05
$N$ (aza)	1.41	1.73	1.82	1.88	1.92	1.95
$C_{\text{meso}}$	0.98	1.08	1.04	0.99	0.93	0.88
$C_\alpha$ (pyr)	1.08	0.78	0.82	0.89	0.97	1.06
$C_\beta$ (pyr)	1.02	1.05	0.99	0.92	0.85	0.77
$N$ (pyr)	1.63	1.79	1.86	1.91	1.94	1.96

TABLE VII: The variation in b.o.s of the porphine bonds with different oxidation states of the central metal ion. B.o.s of bonds for which the value is not quoted can be obtained by imposing  $D_2$  symmetry of the porphine.

Bond	Charge on metal site				
	1	2	3	4	5
$C_\beta - C_\beta$	0.74	0.72	0.69	0.62	0.57
$C_\beta - C_\alpha$	0.47	0.50	0.54	0.59	0.62
$C_\beta - C_\alpha$	0.47	0.51	0.54	0.59	0.62
$C_\alpha - N$	0.41	0.34	0.27	0.22	0.17
$C_\alpha - N$	0.42	0.34	0.27	0.22	0.17
$C_\alpha - C_{\text{meso}}$	0.59	0.60	0.60	0.59	0.57
$C_\alpha - C_{\text{meso}}$	0.59	0.60	0.60	0.59	0.57
$C_\alpha - C_{\text{meso}}$	0.57	0.58	0.59	0.59	0.60
$C_\alpha - C_{\text{meso}}$	0.57	0.58	0.59	0.59	0.60
$C_\beta - C_\alpha$	0.55	0.57	0.58	0.61	0.62
$C_\beta - C_\alpha$	0.54	0.56	0.58	0.60	0.61
$C_\alpha - N$	0.35	0.28	0.22	0.18	0.14
$C_\alpha - N$	0.33	0.27	0.22	0.18	0.14
$C_\beta - C_\beta$	0.61	0.61	0.59	0.56	0.52

decrease sharply. Meso-bonds show minimum change; one set of b.o.s increases while the other set decreases, leading to small alternation in the *meso*-bonds. The asymmetry in the geometry of two rings reduces as the charge on the metal ion increases. The  $C - N$  bonds of aza rings have almost same b.o.s for all oxidation state while in pyrrole rings they are of same magnitude only for higher oxidation states.

Our calculations are in good agreement with earlier semi empirical results. Poveda *et al.* [45] found that  $C_\beta - C_\beta$  bonds are the strongest bonds and the  $C_\beta - C_\alpha$  bonds are the weakest bonds in both Mg Octaethyl tetraphenyl porphyrin (OETPP) and *ZnOETPP*. For charge +2 we also find that the  $C_\beta - C_\beta$  bonds are the strongest bonds and  $C_{\text{meso}} - C_\alpha$  bonds are stronger than  $C_\alpha - C_\beta$  bonds. The C – N bonds become weaker in the presence of the metal ion. All the C – N b.o.s of FBP are always higher than those in the metallo-porphine. Pyrrolic C – N bonds have a slight alternation in bond order pattern at lower oxidation states. FBP in the excited states show alternate b.o.s for C – N bonds either in the aza rings or in the pyrrole rings. While FBP has a 18-annulenic structure, metallo-porphine shows 20-annulene like structure when the charge on the metal ion increases.

## 2. Optical properties

The metallo-porphines have higher symmetry than FBP; former has  $D_{4h}$  point group symmetry while the point group symmetry of the latter is  $D_{2h}$ . Hence the spectra of metallo-porphines have more degenerate excitations than in FBP.

The characteristic optical spectra of metallo-porphines consists of a  $Q$ -band lying between 500-600 nm.  $Q$ -bands have two nearly degenerate levels separated by  $1250\text{ cm}^{-1}$ . It was originally identified as a vibronic progression and assigned  $Q_{0 \rightarrow 0}$  and  $Q_{0 \rightarrow 1}$  transition [46].  $B$ -band which is the most intense band lies between 380 and 420 nm. Other  $L$ ,  $M$  and  $N$  bands are comparatively weak and appear between 325 nm and 215 nm.

The five lowest excitation gaps along with transition dipole moments are given in Table VIII for five different oxidation states of the metal ion. The first allowed state lies about  $\approx 1.70\text{ eV}$  above the gs. For  $q_M = +1$  and  $q_M = +2$  transition dipoles decrease with increasing charge. The lowest level has almost no intensity for dipole transition from gs for  $q_M = +3$  and the second level has significant intensity. We find that for metal ion oxidation states upto  $q_M = +3$ ,  $Q$ -bands are well separated. But with increase in  $q_M$ , the separation between  $Q$ -bands decreases. For  $q_M > +3$  on the metal ion, this separation is very small, and both states have large transition dipoles to the gs although with different polarizations. The intensity for second  $Q$ -band transition for  $q_M = +2$  is weak and is consistent with experimental results [47]. Experiments show that the first excited state of metallo-porphines is slightly lower in energy than in FBP, irrespective of substitutions at the *meso*-positions as shown in reference [48]. There is only a small variation (maximum of  $0.1\text{eV}$ ) in optical gap for different substituents.

From our DMRG results, the strongly optically allowed band,  $B$ -band, lies between  $3.8 \pm 0.2\text{eV}$  above the gs for all values of  $q_M$ . These levels show red shift of about  $0.2\text{eV}$  as  $q_M$  is increased from +1 to +5. For

TABLE VIII: Excitation gaps for singlet-singlet transition of five lowest optically allowed states and transition dipole moments for different metallic charges.

$q_M$	Excited Optical gap		$ \mu $
	state	(in eV)	(in a.u.)
1	1B	1.70	0.80
	2B	2.04	0.08
	3B	3.94	0.66
	4B	4.11	2.30
	5B	5.37	0.26
2	1B	1.69	0.46
	2B	1.97	0.16
	3B	4.00	2.43
	4B	4.22	0.66
	5B	5.36	0.59
3	1B	1.70	0.06
	2B	1.84	0.41
	3B	3.87	2.53
	4B	4.23	0.58
	5B	5.13	0.55
4	1B	1.66	0.66
	2B	1.73	0.71
	3B	3.59	2.41
	4B	4.36	1.38
	5B	5.20	0.40
5	1B	1.65	1.02
	2B	1.68	1.06
	3B	3.62	2.26
	4B	4.31	1.32
	5B	4.78	0.10

$q_M = +2$ , the experimental gaps are about  $3.22\text{eV}$  for Zn and  $3.18\text{eV}$  for Mg(etio)Porphine [47]. Time dependent density functional theory calculation of Minaev *et al.* has a blue shift of  $0.23$  [49], while symmetry adapted cluster CI study of Hasegawa *et al.* has a blue shift of  $0.5\text{ eV}$  for the  $B$  band compared to the experimental results [50]. The blue shift in our DMRG studies is  $0.6\text{ eV}$ . Complete active space second order perturbation theory (CASPT2) calculation of Rubio *et al.* underestimates the experimental excitation energies by  $0.3$  to  $0.5\text{eV}$  [51].

We observe a transition of medium intensity around  $4.2 \pm 0.1\text{ eV}$  in all metallo-porphines, corresponding to experimental absorption peaks for  $N$ -bands of Mg(etio)Porphine and TPPMgP observed at  $3.85\text{eV}$  and  $3.97\text{eV}$  respectively. Our result overestimates this gap by  $\approx 0.3\text{eV}$ . There is also a weak  $L$ -band around  $5.3 \pm 0.1\text{eV}$ . To the best of our knowledge, there are no experimental results for system with  $q_M \geq 3$ , for regular metalloporphines for comparison with DMRG results.

TABLE IX: Triplet state energies, T-T gaps and corresponding transition dipole moments of metallo-porphine for different oxidation state of metal ions.

$q_M$	state index	Triplet energies (eV)	T-T gap (eV)	$ \mu $ (in a.u.)
1	1	3.31	1.29	0.30
	2	3.48	1.46	0.59
	3	4.11	2.09	0.28
	4	4.91	2.89	0.17
2	1	3.01	1.27	0.34
	2	3.33	1.59	0.29
	3	3.84	2.10	0.25
	4	4.41	2.67	0.19
3	1	2.99	1.27	0.19
	2	3.31	1.59	0.08
	3	3.62	1.90	0.47
	4	4.23	2.51	0.12
4	1	3.29	1.69	0.07
	2	3.45	1.85	0.09
	3	3.99	2.39	0.48
	4	4.11	2.51	0.24
5	1	2.76	1.60	0.69
	2	3.25	2.09	0.51
	3	3.30	2.14	0.55
	4	3.73	2.57	0.26

### 3. Triplet-Triplet spectra

In Table IX, triplet energies and triplet-triplet (T-T) gaps and corresponding transition dipole moments are given. Goutermann *et al.* [52] observed a weak T-T absorption at  $1.41\text{eV}$  and a high energy T-T absorption at  $1.58\text{eV}$  with high intensity in case of TPPZn. Sapunov *et al.* observed a peak at  $1.53\text{eV}$  for the same system in dimethyl phthalate solvent [42] while Pileni *et al.* observed peaks at  $1.48\text{eV}$  and  $1.68\text{eV}$  in DODAC solution of TPPZn. Goutermann *et al.* also measured the phosphorescence of  $(TPP)SnCl_2$ , which exhibits similar behavior as TPPZn. DMRG results for  $q_M = 2$  have the first T-T transition at  $1.27\text{eV}$  and the second at  $1.59\text{eV}$ . The first transition is red-shifted compared to the experimental value. In our calculation we observe that the intensity of the first peak is comparable to the second peak. Other higher excited states have relatively weak intensities.

As the oxidation state of the metal ion increases, the first T-T gap remains almost a constant at  $1.27\text{eV}$  up to  $q_M = 3$  and then it increases for charge  $q_M = 4$  and 5. All the T-T gaps for charge  $q_M = +2$  and  $q_M = +3$  are similar. For charge  $q_M = 4$ , the first observable transition is at  $2.39\text{eV}$ . For  $q_M = 5$ , all the T-T transitions have significant transition dipoles.

## V. NONLINEAR OPTICAL PROPERTIES OF PORPHINES

Hitherto, the dynamical NLO response of porphines has been studied using a sum-over-state (SOS) method in conjunction with restricted CI studies. As has been stated before, DMRG method is far superior to other many-body technique for quasi-one-dimensional systems. Besides, the DMRG method has been combined with the CV method to bypass computing only a part of the excited state spectrum as required in the SOS method. The CV method incorporates the full excitation spectrum in the truncated DMRG basis, which in our scheme corresponds to about 45,000 excited states for the DMRG cut-off of  $m = 210$ .

We have calculated the linear and third order nonlinear optic coefficients corresponding to third harmonic generation (THG). These response coefficients have been calculated at three different frequencies. These computational results have been obtained for both FBP and regular metalloporphines.

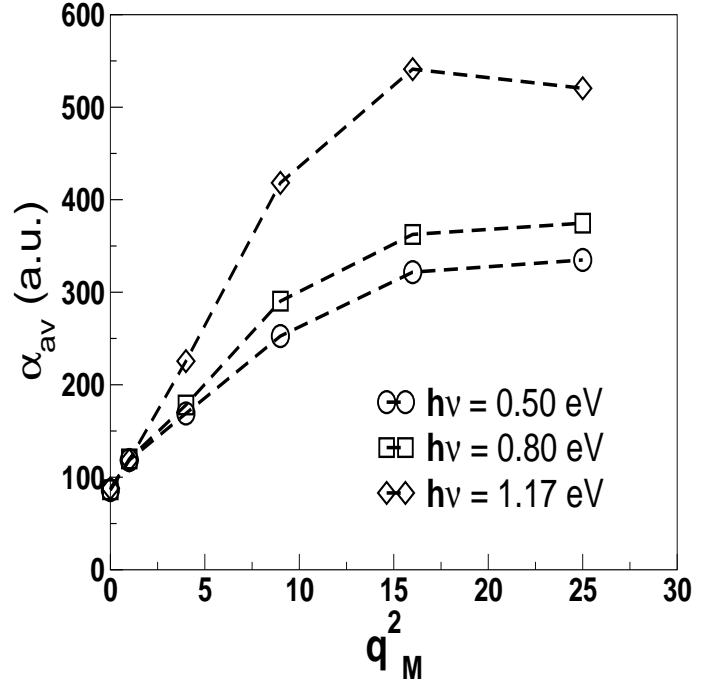


FIG. 6: Tumbling averaged linear polarizability ( $\alpha$ ) vs  $q_m$  at three different frequencies.

For small system sizes (up to about 12 sites), the DMRG calculations can be compared with exact results. This has been done for polarizability  $\alpha$ , as well as for the THG coefficients ( $\gamma$ ) for various components and at dif-

TABLE X: Tumbling averaged THG coefficient  $\gamma_{av}$  in  $10^3$  a.u, for different excitation frequencies and oxidation states of the central metal ion.

$q_M$	$\omega$	Real ( $\gamma$ )	Img( $\gamma$ )
0.0	0.65	158.20	0.00
	0.80	169.51	0.00
	1.17	220.14	0.01
1.0	0.50	1584.88	0.93
	0.80	1276.63	0.04
	1.17	1367.07	1.05
2.0	0.65	1237.32	0.48
	0.8	1122.09	0.20
	1.17	1076.71	0.38
3.0	0.65	1599.05	1.08
	0.80	1220.09	0.30
	1.17	1117.39	0.13
4.0	0.50	2148.68	1.32
	0.80	1711.20	0.18
	1.17	1756.68	0.88
5.0	0.65	3171.83	1.60
	0.80	2719.45	0.32
	1.17	3531.41	4.75

ferent frequencies. The accuracy is typically better than 1% for dominant components away from resonances.

As shown in the Fig. 6, tumbling averaged linear polarizability  $\alpha_{av}$  increases quadratically with increasing oxidation state,  $q_M$ , on the metal ion at all the frequencies we have studied. However, there seems to be saturation in the  $\alpha_{av}$  value for  $q_M > 3$ , at all frequencies. This trend seems to be consistent with the optical gaps and associated transition dipole moments for the low-lying states for different  $q_M$  values, although quantitative in-

ference about  $\alpha_{av}$  cannot be arrived at based on the few low-lying state properties we have computed.

The tumbling averaged THG coefficients ( $\gamma_{av}$ ), are presented in Table X. The THG coefficients, at all the three frequencies we have computed are about one order of magnitude smaller for FBP than regular metallo-porphines. Increase in  $q_M$  leads to increase in  $\gamma_{av}$ , away from resonances.  $\gamma_{av}$  value for  $q_M = 1, 2$  and  $3$  are very similar and much larger than the FBP values. For  $q_M > 3$ , there is a large increase in  $\gamma_{av}$ , with  $q_M$ . Thus metallo-porphines with large oxidation state on the metal ion are expected to exhibit large THG responses.

## VI. CONCLUSION

In Summary, we have employed the symmetrized DMRG method for studying the linear and nonlinear optical properties of FBP and metallo-porphines within an interacting  $\pi$ -electron model. We note that the computed singlet and triplet low-lying excited state energies and their charge densities are in excellent agreement with experimental as well as many other theoretical results. From our bond order calculation, we conclude that porphine has 18-annulenic structure in the ground state and the molecule gets expanded upon excitation. We have modelled the metalloporphine by taking an effective electric field due to the metal ion and computed the excitation spectrum. Metalloporphines have  $D_{4h}$  symmetry and hence more degenerate excited states. The ground state of Metalloporphines show 20-annulenic structure, as the charge on the metal ion increases. The linear polarizability seems to increase with the charge initially and then saturates. The same trend is observed in third order polarizability coefficients.

**Acknowledgments.** MK thanks UGC India for financial support. SR thanks DST India for funding through different programmes.

- 
- [1] K. S. Suslick, N. A. Rakow, M. E. Kosal, and J-H. Chou, J. Porphyrins and Phthalocyanines, **4**, 407 (2000).
  - [2] D. A. Parthenopoulos, and P. M. Rentzepis, Science, **245**, 843 (1989).
  - [3] J. E. Ehrlich, X. L. Wu, I.-Y. S. Lee, Z.-Y. Hu, H. Röckel, S. R. Marder, and J. W. Perry, Opt. Lett., **22** 1843 (1997).
  - [4] K. S. Suslick, S. V. D-Jeffries, In *Comprehensive Supramolecular Chemistry: Bioinorganic Systems*, **5**, by Ed. K. S. Suslick, 733 (1996).
  - [5] T. S. Mang, T. J. Dougerty, W. R. Potter, D. G. Boyle, S. Sommer, and J. Moan, Photochem. Photobiol., **45**, 501 (1987).
  - [6] S.-Y. Wong, R. W.-Y. Sun, N. P. -Y. Gratzel Chung, C.-L. Lin, and C.-M. Che., Chem. Commun., **28**, 3544 (2005).
  - [7] Md. K. Nazeeruddin, R. H. Baker, D. L. Officer, W. M. Campbell, A. K. Burrell, and M. Gratzel, Langmuir, **20**, 6514 (2004).
  - [8] M. Cinchetti, S. Neuschwander, A. Fischer, A. Ruffing, S. Mathias, J. Wstenberg and M. Aeschlimann, Phys. Rev. Lett., **104**, 217602 (2010); M. Cinchetti, K. Heimer, J. Wstenberg, O. Andreyev, M. Bauer2, S. Lach1, C. Ziegler, Y. Gao and M. Aeschlimann, Nature Materials **8**, 115 (2009).
  - [9] S. Stepanow, A. Mugarza, G. Ceballos, P. Moras, J. C. Cezar, C. Carbone, and P. Gambardella, Phys. Rev. B **82**, 014405 (2010).
  - [10] C. Isvoranu, B. Wang, K. Schulte, E. Ataman, J. Knudsen, J. N. Andersen, M. L. Bocquet and J. Schnadt, J. Phys. Condens. Matter, **22**, 472002 (2010).
  - [11] N. Atodiresei, V. Caciuc, P. Lazic, S. Blgel, Phys. Rev. Lett. **102**, 136809 (2009); N. Atodiresei, J. Brede, P. Lazic, V. Caciuc, G. Hoffmann, R. Wiesendanger, S. Blgel, Phys. Rev. Lett. **105**, 066601 (2010).

- [12] M. Goutermann, J. Mol. Spectrosc., **6**, 138 (1961); M. Goutermann, in *The Porphyrins*, Ed. by D. Dolphin, Academic Press, New York, Part A (1978).
- [13] C. Weiss, H. Kobayashi and M. Goutermann, J. Mol. Spectr., **16**, 415 (1965).
- [14] J. D. Petke, G. M. Maggiora, L. L. Shipman and R. E. Christoffersen, J. Mol. Spectr., **71**, 64 (1978).
- [15] W. D. Edwards and M. C. Zerner, Int. J. Quant. Chem., **23**, 1407 (1983).
- [16] K. A. Nguyen, P. N. Day and R. Pachter, J. Phys. Chem. A., **104**, 4748 (2000).
- [17] S. Priyadarshy, M. J. Therien and D. N. Beratan, J. Am. Chem. Soc., **118**, 1504 (1996).
- [18] I. D. L. Albert, T. J. Marks and M. A. Ratner, Chem. Mater., **10**, 753 (1998).
- [19] J. S. Shirk, R. G. S. Pong, S. R. Flom, F. J. Bartoli, M. E. Boyle, and A. W. Snow, Pure Appl. Opt., **5**, 701 (1996).
- [20] X. Zhou, A.-M Ren, J.-K. Feng, X.-J. Liu and Y.-D. Zhang, Chem. Phys. Chem, **4**, 991 (2003).
- [21] P. C. Ray, and Z. Sainudeen, J. Phys. Chem., A **110**, 12342 (2006).
- [22] S. R. White, Phys. Rev. Lett., **69**, 2863 (1992).
- [23] Jeckelmann, E., and S. R. White, Phys. Rev. B **57**, 6376 (1998).
- [24] Y. Anusooya, Swapan K. Pati, S. Ramasesha, J. Chem. Phys., **106**, 10230 (1997).
- [25] C. Raghu, Y. Anusooya Pati, and S. Ramasesha, Phys. Rev. B, **66**, 035116 (2002).
- [26] Manoranjan Kumar and S. Ramasesha, Phys. Rev. B **81**, 035115 (2010).
- [27] Manoranjan Kumar, S. Ramasesha, and Z. G. Soos Phys. Rev. B **79**, 035102 (2009).
- [28] R. Chitra, Swapan K. Pati, H. R. Krishnamurthy, Diptiman Sen, and S. Ramasesha, Phys. Rev. B **52**, 5681 (1995).
- [29] T. Xiang, J. Lou, and Z. Su Phys. Rev. B **64**, 104414 (2001).
- [30] Manoranjan Kumar, S. Ramasesha, Diptiman Sen, and Z. G. Soos Phys. Rev. B **75**, 052404 (2007).
- [31] U. Schollwck, The density-matrix renormalization group, Rev. Mod. Phys. **77**, 259 (2005).
- [32] S. Ramasesha, S. K. Pati, Z. Shuai, and J. L. Brdás, Adv. Quantum Chem., **38**, 121 (2001).
- [33] L. E. Webb and E. B. Fleischer, J. Am. Chem. Soc., **87**, 668 (1965).
- [34] K. Ohno, Theor. Chim. Acta, **2**, 219 (1964).
- [35] Z.G. Soos, Chem. Phys. Lett., **153**, 171 (1988) and Z. G. Soos and S. Ramasesha, J. Chem. Phys., **90**, 1067 (1989).
- [36] Z. G. Soos and S. Ramasesha, J. Chem. Phys., **92**, 5166 (1990).
- [37] S. Ramasesha, J. Comput. Chem., **11**, 545 (1990).
- [38] Swapan K. Pati, and S. Ramasesha, Z. Shuai and J. L. Brédas, Phys. Rev. B **59**, 14827 (1999).
- [39] C.-Kui Wang, Peter Macak, Yi Luo, and Hans Ågren, J. Chem. Phys., **111**, 9813 (2001).
- [40] C. Rimington, S. F. Mason, and O. Kennard, Spectrochim. Acta, **12**, 65 (1958).
- [41] D. H. Dolphin, M. Goutermann and A. D. Adler: J. Mol. Spectr., **38**, 16 (1971).
- [42] V.V. Sapunov, K.N. Solovév, M.P. Tsvirko, Zh. Prikl. Spektrosk. **21**, 667 (1974); **111**, 6500 (1989).
- [43] I. Carmichael, , H. L. Gordon, J. Phys. Chem., **15**, 1 (1986).
- [44] W. T. Simpson, J. Chem. Phys., **17**, 1218 (1949).
- [45] L. A. Poveda, V. R. Ferro, J. M. Garcia de la Vega and R. H. Gonzalez-Jonte, Phys. Chem. Chem. Phys., **2**, 4147 (2000).
- [46] J. R. Platt, in *Radiation Biology* Ed. by A. Hollaender, Chapter-2, McGraw-Hill, New York, (1956).
- [47] M. Goutermann, J. Chem. Phys., **30**, 1139 (1959); J. Mol. Spectr. **6**, 138 (1961); M. Goutermann, G. H. Wagnière, and L. C. Snyder, J. Mol. Spectr., **11**, 108 (1963).
- [48] J. Rodriguez, C. Kirmaier and D. Holten, J. Am. Chem. Soc., **111**, 6500 (1989).
- [49] B. Minaev and H. Ågren, Chem. Phys., **315**, 215 (2005).
- [50] J. Hasegawa, M. Hada, M. Nonoguchi, and H. Nakatsuj, Chem. Phys. Lett., **250**, 159 (1996).
- [51] L. Andrés, M. Merchána, M. Rubio and Björn O. Roos, Chem. Phys. Lett., **295**, 195 (1998).
- [52] M. Goutermann and G.E. Khalil, J. Mol. Spectr., **53**, 88 (1974).
- [53] X. Wang, L. J. Kerbs, H. E. Pudavar, S. Ghosal C. Liebow, A. V. Schally and P. N. Prasad, Proc. Natl. Acad. Sci., **96** 11081 (1999).
- [54] M. P. Joshi, H. E. Pudavar, J. Swaitkiewicz, P. N. Prasad, B. Reianhardt, Appl. Phys. Lett., **74** 170 (1999).
- [55] S. Kawatta, Y. Kawatta, Chem. Rev., **100** 1777 (2000).
- [56] J. Rodriguez, C. Kirmaier and D. Holten, J. Am. Chem. Soc., **111** 6500 (1989).
- [57] R.L. Goyan and D.T. Cramb, Photochem. Photobiol., **72** 821 (2000).
- [58] D.T. Cramb and R.L. Goyan, Proc. SPIE, **4262** 41 (2001).
- [59] M. Drobizhev, A. Karotki and A. Rebane, Chem. Phys. Lett., **334** 76 (2001).
- [60] M. Drobizhev, A. Karotki, M. Kruk and A. Rebane, Chem. Phys. Lett., **355** 175 (2002).